JOURNAL OF CATALYSIS **168,** 245–254 (1997)
ARTICLE NO. CA971618

Chromia- and Chromium Sulfide-Pillared Clays: Preparation, Characterization, and Catalytic Activity for Thiophene Hydrodesulfurization

Mikhail Sychev,* V. H. J. (San) de Beer,† Alexander Kodentsov,† Eugene M. van Oers,† and Rutger A. van Santen†

*Faculty of Chemical Technology, Kiev Polytechnic Institute, 14-40 TNV, Pr. Peremogy 37, 252056 Kiev-56, Ukraine; and †Schuit Institute of Catalysis, Eindhoven University of Technology, PO Box 513, 5600 MB Eindhoven, The Netherlands

Received August 1, 1995; revised January 2, 1997; accepted January 20, 1997

Chromia-pillared clay has been synthesized from naturally occurring montmorillonite through exchange of interlamellar ions with hydroxychromium polycations. Sulfidation of the heat-treated precursor with an H_2S–H_2 mixture at 673 K results in the formation of chromium sulfide-pillared clay. The materials were characterized by X-ray diffraction, thermogravimetric analysis, nitrogen adsorption, scanning electron microscopy, electron probe microanalysis, and X-ray photoelectron spectroscopy. These methods showed that heat treatment of chromia-pillared clay under the conditions applied did not drastically change the pore structure or the chromium oxidation state and the distribution of pillars, but strongly influenced its aggregate morphology. Sulfide-pillared material has an interlamellar distance of 1.01 nm, a BET surface area of 256 $m^2\ g^{-1}$, a micropore volume of 0.082 $cm^3\ g^{-1}$, and a pore slitwidth of 1.24 nm. The sulfidation procedure does not significantly change the pillared structure or the chromium oxidation state. Sulfur is found to be present as practically uniformly distributed S^{2-} species. The chromium sulfide phase in the finely dispersed and well-distributed state that is reached in sulfide-pillared clay is of primary importance to the high thiophene conversion over this catalyst. In the presence of this catalyst, thiophene hydrodesulfurization results exclusively in the formation of butane and butene. The distribution of hydrocarbons depends on the reaction temperature, with a higher butane yield at lower temperature.

INTRODUCTION

Transition metal sulfides (TMSs) are used extensively as hydrotreating catalysts. Their great importance is reflected in the amount of published literature on this subject (1–3). These catalysts are prepared in oxide form, although the active phase during the catalytic action is a sulfided one. In hydrodesulfurization (HDS) and hydrocracking, TMS catalysts supported on zeolites are more active than those supported on silica–alumina or alumina (4, 5). Pillar interlayered clays (PILCs) possess some properties comparable to those of the zeolites. Their pore structure and catalytic behavior can be varied over a wide range by changing the type of intercalate (6–8). Therefore, such materials containing Group VI and VIII transition metals have potential application in hydrotreatment. PILCs are formed by incorporation of large polymeric or oligomeric hydroxycations into the interlamellar space of smectite clays (e.g., montmorillonite) through ion exchange (6). The resultant materials, after heat treatment, contain oxide clusters (pillars) that maintain the lattice expansion, even at high temperatures, and thus expose the internal surface of clay layers. The cavities so formed are easily accessible for adsorption of gases and vapors. Moreover, the metal oxide pillars can be modified by oxidation/reduction to become catalytically active.

Only a few data concerning metal sulfides supported on pillared clays have been reported. Fe sulfide-pillared montmorillonite was first prepared by Burch and Warburton (9) to be used for high-pressure demetallization of heavy crude oil (10); however, the product obtained was highly interstratified (11). Occelli and Rennard (12) applied pillared bentonite as a support for Ni–Mo catalysts for the hydrogenation–hydrocracking of vacuum gas oil feedstocks. In both cases the catalysts demonstrated interesting catalytic properties. Kloprogge *et al.* (13) reported that nickel sulfide supported on Al-pillared montmorillonite exhibits high thiophene HDS activity.

Chromia-pillared montmorillonite exhibits high activity and selectivity in cyclohexane dehydrogenation, hydrocracking of *n*-decane (14, 15), and toluene disproportionation (16), as well as dehydrogenating properties in cumene conversion (17). Chromia-pillared clay activated with an H_2S–H_2 mixture displayed interestingly high activity for thiophene HDS and consecutive hydrogenation of butene (18).

Most of the early attempts to incorporate oligomeric chromium ions into the interlamellar space of smectite made use of chromium salt solution hydrolyzed at room temperature (19); however, the materials obtained by this method have a basal spacing of only 1.68 nm. Therefore, Pinnavaia *et al.* (15) proposed the use of elevated

0021-9517/97 $25.00

temperatures for the pillaring reagent formation and for the ion-exchange reaction. As a result, Cr-PILCs with a basal spacing of 2.5 to 2.7 nm and a BET surface area of 353 to 433 $m^2\ g^{-1}$ were synthesized. These values are much larger than those for typical alumina-pillared clays (1.6–1.8 nm) (7). Auer and Hofmann (16) reported that such chromia-pillared clays had stronger Lewis acid sites than alumina- and zirconia-pillared clays. The authors found that the number of those sites correlated with the number of pillars. Recently, Cr-PILCs were synthesized by *in situ* hydrolysis of chromium acetate on the montmorillonite surface (20). By this method Cr-PILCs with a BET surface area ranging from 366 to 464 $m^2\ g^{-1}$ and narrow pore size distributions centered between 0.75 and 1.20 nm can be prepared. Thermally stable chromia-pillared montmorillonite materials were obtained on calcination under ammonia up to 898 K (20).

The objectives of the present study are to (1) investigate some details of chromia-pillared montmorillonite synthesis, (2) determine the properties of chromium sulfide clay, and (3) screen the activity of this catalyst in thiophene HDS. To accomplish the characterization, X-ray diffraction (XRD), thermogravimetric (TG) analyses, N_2 adsorption, X-ray photoelectron spectroscopy (XPS), scanning electron microscopy (SEM), and electron probe microanalysis (EPMA) were used.

EXPERIMENTAL

1. Preparation

The pillaring reaction of the clay was performed following a procedure described elsewhere (18) which is similar to the method proposed by Tzou (14). The pillaring agent containing hydroxychromium polycations was formed by heating a 0.10 *M* solution of chromium nitrate with Na_2CO_3 at 368 K for 36 h. Prior to this, solid Na_2CO_3 was gradually added to a vigorously stirred $Cr(NO_3)_3$ solution at room temperature so that the molar ratio of hydroxide to chromium ions equaled 2.0. The starting material, viz., purified natural Oglanlinsky montmorillonite (CIS), is described elsewhere (21). It was first transformed to the Na form (22). The fraction of this cationic form with particle sizes $<2\ \mu$m collected by sedimentation was added slowly as an aqueous suspension (1 wt%) to a vigorously stirred pillaring agent at 313 K, and the mixture was stirred for 1.5 h. Chromium was present in great excess, typically 50 mmol Cr^{3+}/meq clay. The products were repeatedly centrifuged and washed with deionized water until flocculation occurred, usually 12 times. The resulting material was then air-dried on a glass plate at room temperature (referred to as Cr-PM) and heat-treated in a thin-bed configuration under He flow [referred to as Cr-PM(He)]. The temperature during this operation was raised at 50 K h^{-1} and maintained for 5 h at 673 K. Sulfided samples were prepared in a H_2S/H_2 flow (10 mol% H_2S, 60 ml min^{-1}) using the following temperature program: 6 K min^{-1} heating rate from 293 to 673 K and 2 h at 673 K [referred to as Cr-PM(sulf)]. For comparative purposes, a sample of homoionic Cr^{3+} montmorillonite was prepared by repetitive ion exchange in a 1 *M* $CrCl_3$ aqueous solution followed by centrifugation and washing until chlorine free.

2. Characterization

a. X-ray diffraction. Since pillared clays usually show broad XRD patterns, the use of oriented specimens is helpful for the basal spacing determination. Such specimens were prepared by allowing a 1 wt% slurry of the flocculated material mentioned above to dry in air at 313 K on a glass slide. The same procedure was applied to the preparation of specimens from heat-treated and sulfided materials. The XRD patterns were obtained on a Philips PW 1120 diffractometer using Ni-filtered monochromatized Cu $K\alpha$ radiation and the stepscan method for peak registration.

b. Thermogravimetric analysis. TG-DTG analyses were performed with a Setaram TG 85 thermobalance by heating a 40-mg sample at 6 K min^{-1} from 293 to 1073 K in a helium flow (30 ml min^{-1}).

c. Surface area and pore structure. BET surface area and pore structure were derived from nitrogen adsorption–desorption isotherms determined at 77 K (degassing at 393 K, 10^{-4} mbar, 5 h) using a conventional volumetric apparatus (Sorptomatic 1900, Carlo Erba Instruments).

d. X-ray photoelectron spectroscopy. X-ray photoelectron spectra of air-dried and heat-treated samples (fresh or sulfided) were obtained with a VG ESCALAB 200 MK photoelectron spectrometer equipped with the twin-anode Al $K\alpha$ source (1486.6 eV), a hemispherical analyzer with a five-channel detector operating at a pass energy of 20 eV at room temperature and at a pressure lower than 6.5×10^{-9} mbar.

Sulfided samples were prepared as described above. After sulfidation the catalysts were purged with purified He for 30 min at 673 K and subsequently cooled to room temperature in flowing He. A special reactor was used that allowed transfer of the sulfided samples to the XPS apparatus through a recirculation-type glove box (N_2: <2 ppm O_2 and H_2O). The samples were analyzed as powder pressed in indium foil. The binding energies were calculated with respect to the C 1*s* peak set at 284.6 eV. The X-ray photoelectron spectra were resolved into their Gaussian-Lorentz components after background subtraction following the Shirley method (23). From the peak areas and sensitivity factors [calculated using cross sections given by Scofield (24)] Cr/Si and S/Cr intensity ratios were determined.

e. Scanning electron microscopy and electron probe microanalysis. Air-dried Cr-PM (oriented thin film) samples

were prepared by sedimentation on a graphite monolith substrate at 313 K. A flocculated aqueous suspension having a Cr-PM concentration of about 1 wt% was used for this purpose. One part of these samples was measured as such. A second part was first heat-treated in a He flow (for conditions, see Section 1). A third part was additionally sulfided in a H_2S/H_2 gas mixture (for conditions, see Section 1). Prior to the scanning electron microscopy (SEM) and EPMA measurements the samples were coated with carbon to achieve sufficient electrical conductivity. A JEOL 840 scanning electron microscope equipped with the a Tracer Northern X-ray energy-dispersive spectrometer (EDS) was employed.

f. Analyses. Besides EPMA, X-ray fluorescence (XRF) analysis and atomic absorption spectroscopy (AAS) (Perkin–Elmer 3030 spectrometer) were used to determine chromium content in the materials studied. For AAS, the samples were completely fused with lithium metaborate at 1273 K and subsequently dissolved in a mixture of 30 ml 3% HNO_3 and 5 ml 15% HCl.

3. Catalytic Activity Measurements

Thiophene HDS activities were measured at 623 and 673 K in a microflow reactor (1 atm, 4.0% thiophene in H_2, 50 cm^3 min^{-1}). Catalyst samples (0.20 g) were sulfided *in situ* under the conditions mentioned in Section 1. Reaction products were analyzed every 35 min by on-line gas chromatography. First-order rate constants for thiophene conversion to hydrocarbons (k_{HDS}) and the consecutive hydrogenation of butene (k_{HYD}) were calculated as described elsewhere (25).

RESULTS AND DISCUSSION

1. X-Ray Diffraction Patterns

The parent Na-montmorillonite has a basal spacing $d(001)$ of 1.29 nm. After pillaring, a broad reflection centered at 6.74 2Θ is observed in the pattern for the non-washed material, as shown in Fig. 1A. This is indicative of irregular basal spacing that leads to some Bragg scattering along the *c* dimension (22). A first (in some cases second) washing results in a second peak positioned at 3.83 2Θ corresponding to a basal spacing of 2.30 nm. This reflects the formation of expanded interlayer space due to the pillaring. It is noteworthy that the intensity of the 001 reflection increases when washing is continued (Fig. 1A, patterns 2 and 3), indicating better structural organization and distribution of the pillars between the clay sheets (11). As stated by Rightor *et al.* (11) this is most likely to be due to hydrolysis of the surface-bound polycations. In view of the considerable impact of washing, all Cr-PM samples were washed 12 times prior to air-drying. Pillared montmorillonite with 25.5 wt% chromium (established by methods mentioned under Experimental) was used for further investigations.

Typical XRD patterns of air-dried, heat-treated, and sulfided chromia-pillared montmorillonite samples are shown in Fig. 1B. The XRD pattern of air-dried material was similar to that previously published (14, 18) and exhibits a reflection corresponding to an enlarged basal spacing at 3.31 2Θ. When Cr-PM samples were heat treated in He flow at 673 K the $d(001)$ value decreased from 2.67 nm at room temperature to 2.15 nm at 673 K (see Fig. 1B, patterns 1 and 2). This is most probably caused by the conversion of hydroxychromium polycations to chromia pillars as result

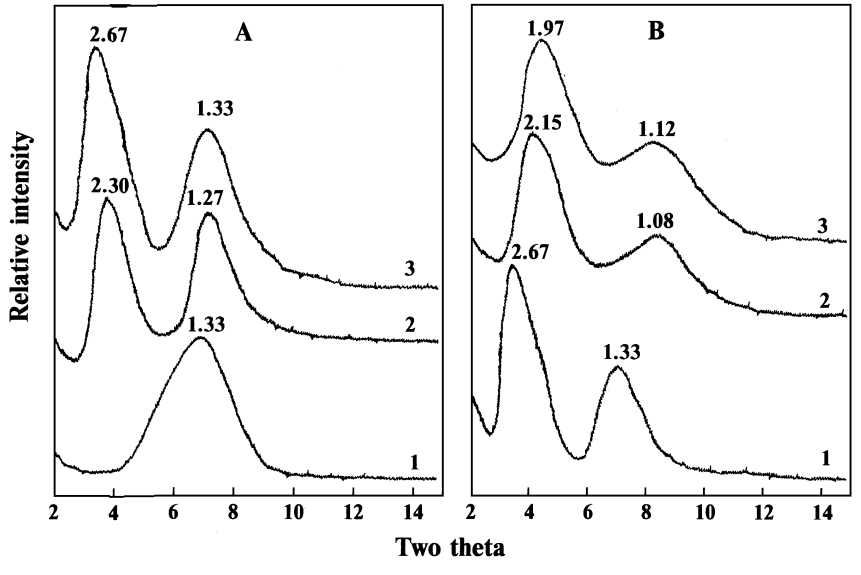

FIG. 1. X-ray diffraction patterns of Cr-PM: (A1) just after pillaring, (A2) after a first washing, (A3) after 12 washings; (B1) air-dried, (B2) heat-treated at 673 K, (B3) sulfided at 673 K.

of dehydration and partial dehydroxylation (26). In the case of homoionic Cr^{3+}-exchanged clay (reference material), heat treatment under the same conditions results in a collapse of the basal spacing. Such behavior was to be expected since thermally stable enlarged interlayering is created by hydroxychromium polycations with molecular dimensions. From the above results it is clear that polymeric cations were indeed formed by the procedure used to prepare pillaring agent. Concerning sulfidation, it can be stated that such treatment does not significantly influence basal spacing. As shown in Fig. 1B (pattern 3), sulfided Cr-PM possesses an enlarged gallery with a height of about 1.01 nm (estimated by subtracting from the basal spacing the thickness of the silicate layer, 0.96 nm); however, both heating and sulfidation treatments result in broadening and intensity decrease of the XRD reflections, as can be seen in Fig. 1B.

2. *Thermogravimetric Analysis*

The thermal behavior of the materials prepared was further investigated using TG analysis. The TG and DTG profiles are shown in Fig. 2. The air-dried chromia-pillared clay exhibits a continuous weight loss of about 24 wt% between 323 and 698 K (Fig. 2A, curve 1) and the three DTG maxima (Fig. 2B, curve 1). This weight loss and the peaks near 363 and 498 K can be attributed to the removal of interlayer water and water coordinated to the hydroxychromium oligomers. The 498 K peak is not present in the DTG profile of Cr^{3+}-exchanged montmorillonite, as follows from Fig. 2, curve 2, and is therefore related to the pillaring phase. In addition, Cr-PM exhibits a less pronounced and broad weight loss (about 3 wt%) between 698 and 923 K and an ill-defined DTG peak at 810 K, which most probably reflects the dehydroxylation of pillars. It is noteworthy that in Cr-PM, dehydroxylation takes place at lower temperatures than in nonpillared Cr-exchanged montmorillonite. For this sample, dehydroxylation occurs within the temperature range 823 to 973 K (Fig. 2B, curve 2). The thermal behavior of the sulfided Cr-PM is different from that of heat-treated precursor, as can be seen in Fig. 2. The ill-defined DTG peak with a maximum at about 923 K (see Fig. 2A, curve 4) probably reveals the transformation of the chromium sulfide phase on heat treatment.

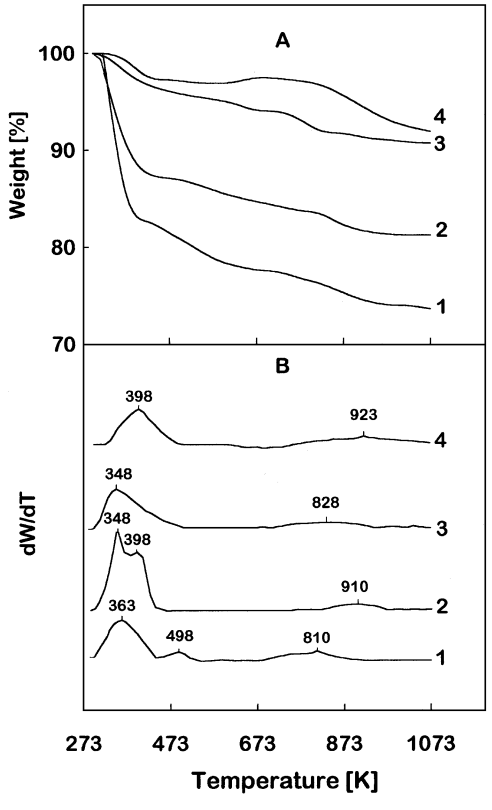

FIG. 2. (A) TG profiles of (1) Cr-exchanged montmorillonite, (2) air-dried Cr-PM, (3) Cr-PM heat-treated at 673 K, and (4) Cr-PM sulfided at 673 K. (B) DTG profiles of (1) Cr-exchanged montmorillonite, (2) air-dried Cr-PM, (3) Cr-PM heat-treated at 673 K, and (4) Cr-PM sulfided at 673 K.

3. *Scanning Electron Microscopy and Electron Probe Microanalysis*

SEM and EPMA were used to study the effect of heat treatment and sulfidation on the Cr-PM aggregation state as well chromium distribution.

The air-dried material exhibits nearly platelike morphology and a distinctively lamellar structure (Fig. 3A). This can be attributed to the face-to-face fashion in which the pillared clay particles stack as a result of drying (27). Cr^{3+}-exchanged montmorillonite shows a folded surface texture (see Fig. 3B). Thus, the pillaring of montmorillonite with hydroxychromium polycations leads to the formation of a more platelike texture than that of the respective cationic form of the clay.

After heat treatment the Cr-PM aggregates become more compact (Fig. 3C). Heat treatment also causes significant disordering of the face-to-face stacking structure, most likely beause of edge-to-face and/or edge-to-edge interactions. This is revealed by the appearance of the delaminated aggregates (27) in the face-to-face associated microstructure. The tendency of chromia-pillared montmorillonite toward delamination has recently been pointed out by Auer and Hofmann (16).

In view of the similar preparation of the specimens for XRD and SEM, it is reasonable to compare results obtained by these two methods. As shown above, heating of Cr-PM leads to broadening and intensity decreases of the XRD reflections because of the weakness of Bragg scattering along the *c* dimension. The same material contains a certain amount of disordered aggregates, as can be seen in Fig. 3C. This implies that variations in Cr-PM aggregate morphology on heating (resulting from partial delamination) affect

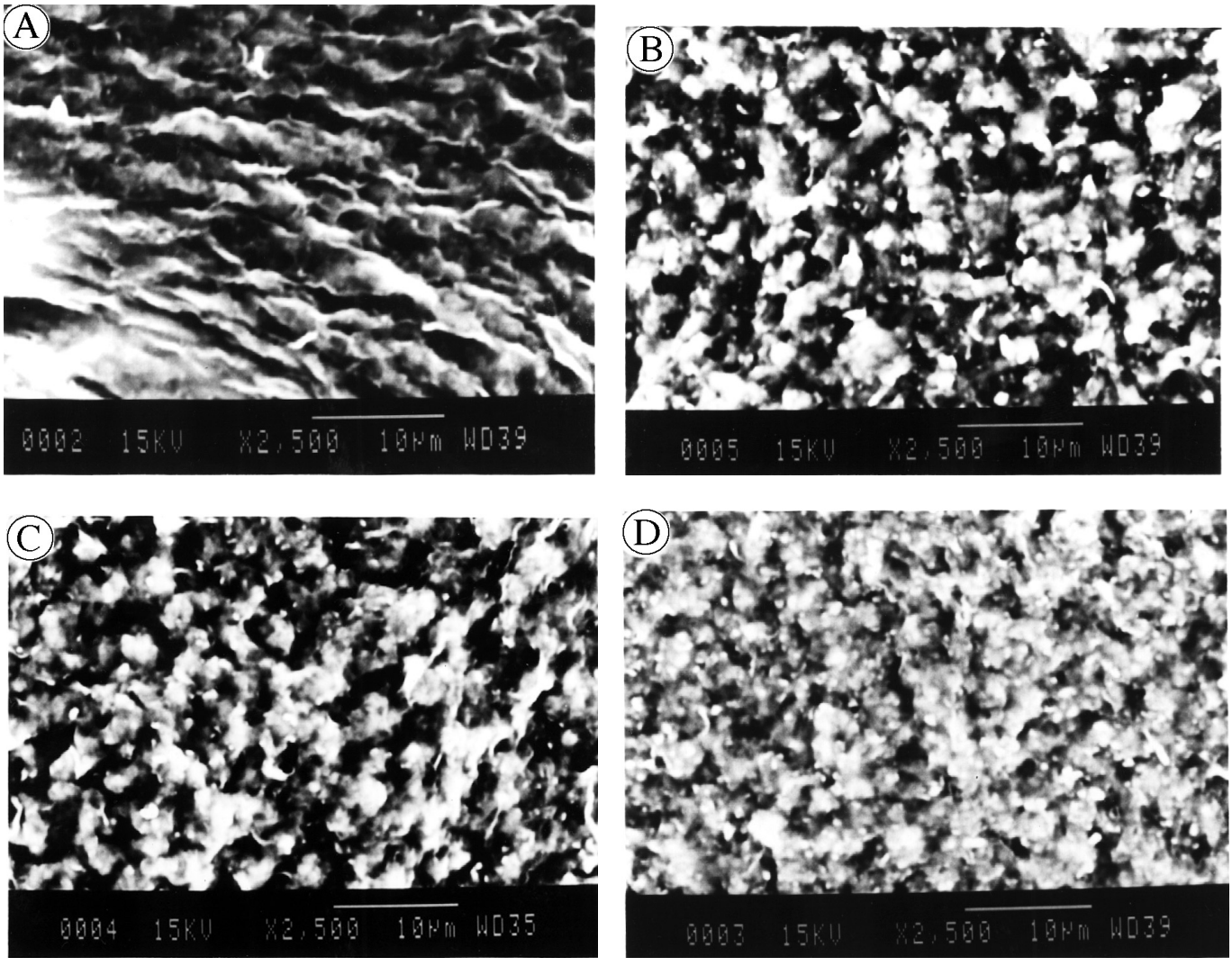

FIG. 3. SEM images of Cr-PM sample: (A) air-dried, (C) heat-treated at 673 K, (D) sulfided at 673 K, and (B) Cr-exchanged montmorillonite.

the width and intensity of the XRD peaks; however, the fraction of delaminated layers in heat-treated product cannot be determined by XRD. Sulfidation of heat-treated Cr-PM results in further disordering of the face-to-face stacking, as shown in Fig. 3D.

To examine the influence of heating and sulfidation on the pillar location in the Cr-PM structure, distribution maps of the $K\alpha$ X-ray radiation of chromium and silicon were studied. These show the practically uniform distribution of characteristic X-ray radiation of these elements on a micrometer-length scale. This underlines that heat treatment does not significantly influence the spatial location of the chromia pillars inside the intercrystalline pore system. In addition, no substantial changes were found in the chromium distribution after sulfidation of Cr-PM(He). The Cr/Si ratio measured by EPMA in heat-treated and sulfided samples is practically the same as in air-dried material. Furthermore, the map of X-ray radiation obtained for sulfur also shows uniform distribution of this element.

4. Nitrogen Adsorption

BET surface area and pore structure of the materials studied were evaluated by this method. Figure 4 shows the nitrogen adsorption–desorption isotherms and Table 1 gives details of the textural properties. The relative pressure region 0.05 to 0.30 was used to calculate BET surface area (7). The N_2 adsorption isotherm for the Cr-PM sample is almost of Type I (Fig. 4, isotherm 1) in the BDDT classification (28) which is characteristic of microporous solids. The observed high value of the C_{BET} parameter (see Table 1) is in line with the microporous texture of the air-dried Cr-PM (20). In addition, the t plot (see Fig. 5) reveals a large micropore contribution. The micropore volume calculated

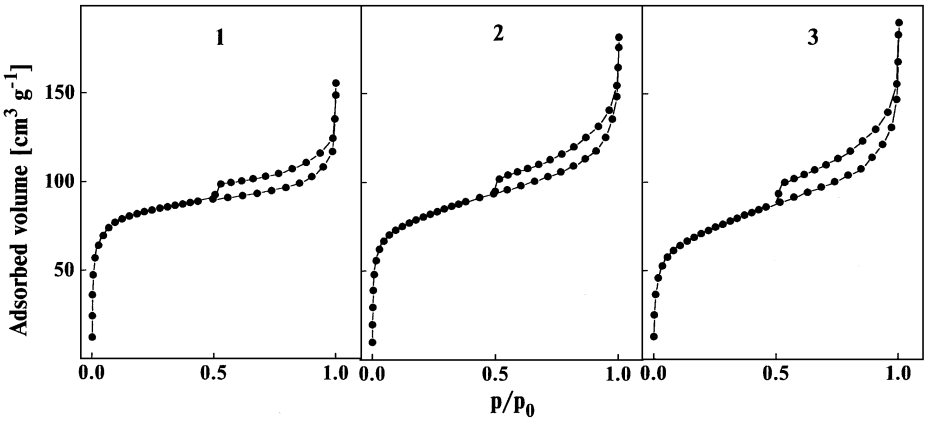

FIG. 4. Adsorption–desorption isotherms for nitrogen on the Cr-PM sample: (1) air-dried, (2) heat-treated at 673 K, (3) sulfided at 673 K.

from the *t* plot (ca. 0.12 cm^3 g^{-1}) is close to that of other pillared montmorillonites (7, 20). The approximate width of the slit-shapped pores [which are characteristic of pillared clays (29)] can be estimated from the inflection point of the *t* plot by multiplying the *t* value corresponding to this inflection point by a factor of 2 (7). The results thus obtained are shown in Table 1. The air-dried Cr-PM has a pore slitwidth of about 0.97 nm. Although air-dried Cr-PM is predominantly microporous, it also exhibits some mesoporosity as indicated by the hysteresis loop at a higher relative pressure (Fig. 4, isotherm 1). The shape of the N_2 desorption isotherm (see Fig. 4, isotherm 1) is almost of Type H4 in the IUPAC classification (30). Among materials displaying this type of hysteresis are those in which the pore structure is composed of parallel plates (29). This finding is in agreement with the textural structure that is to be expected when clay layers are expanded by means of pillaring.

On heat treatment of Cr-PM at 673 K the general shape of the N_2 adsorption isotherm changes only slightly (still almost Type I). In parallel with this the micropore volume, C_{BET} parameter, and surface area decrease somewhat (see Fig. 4, isotherm 2 and Table 1). Assuming that these effects can be explained by complete closure of some pores (31) the main part of the decrease in total surface area can be ascribed to strong collapse of the layers in the unpillared fraction in Cr-PM, the presence of which cannot be excluded. Alternatively, the BET surface area diminution on heating Cr-PM can be attributed to the thermal instability of the montmorillonite sheets caused by hydrolysis of the octahedral cations resulting from the protonic attack (26). This leads to the creation of the disturbed fragments in clay layers of the pillared material which in turn generate the collapsed phase having a low surface area. Summarizing, it can be stated that both elucidations are relevant. Heat treatment results in a partial increase in pore slitwidth, as shown in Table 1. Recently, a similar observation was reported by Malla and Komarneni for alumina-pillared hectorite (32). The authors explained this fact as a change in the interpillar distance caused by pillar dehydration. Indeed, heating results in significant dehydration of the pillared clay, as seen from TG data. Consequently, this process may in fact influence interpillar distance and, therefore, the slitwidth of pores.

Also, sulfidation of Cr-PM has only a small effect on the shape of the N_2 adsorption isotherm (Fig. 4; isotherm 3); however, it causes a further decrease in surface area,

TABLE 1

Surface Areas (BET), Total (V_p) and Micropore (V_m) Volumes, C_{BET} Parameters, and Slitwidths of Pores (2*t*) for Air-Dried and Modified Cr-PM

Sample	S_{BET} (m^2/g)	C_{BET}	V_p (cm^3/g)	V_m (cm^3/g)	2*t* (nm)
Cr-PM	307	599	0.24	0.117	0.97
Cr-PM(He)	293	500	0.28	0.097	1.18
Cr-PM(sulf)	256	264	0.29	0.090	1.24

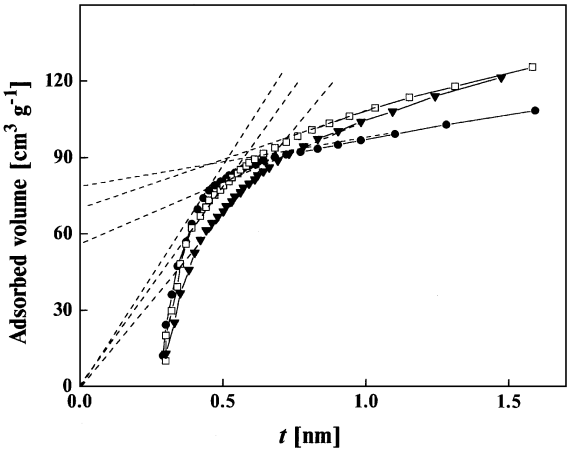

FIG. 5. *t* Plots of nitrogen adsorption isotherms of Cr-PM sample: (●) air-dried (□) heat-treated at 673 K, (▼) sulfided at 673 K.

micropore volume, and C_{BET} parameter and some increase in pore slitwidth (Table 1).

As is known (33), the microporosity of pillared clays is created by incorporation of hydroxymetal polycations into the interlayer space. Therefore, the micropore volume decrease of Cr-PM may reflect the sintering of chromia pillars on heating or sulfidation; however, taking into consideration that the changes of the surface area and micropore volume are relatively small (Table 1), it is reasonable to assume that the degree of such sintering is low as well. This indicates that formation of the metal-sulfide phase takes place not on the external surface but inside the intercrystalline pore system, as result of the reaction between the pillars and the sulfiding agent. Moreover, as can be seen in Table 1, heat treatment and sulfidation of Cr-PM result in a total pore volume increase, probably as a result of the formation of the partially delaminated aggregates in the Cr-PM(sulf) sample, the existence of which determined by SEM and XRD.

Hence, the N_2 adsorption data clearly show that heating and sulfidation do not drastically modify the pore structure of chromia-pillared montmorillonite which persists with virtually no collapse.

5. *X-Ray Photoelectron Spectroscopy*

The oxidation states of chromium and transformation of pillars on heat treatment and sulfidation of Cr-PM were further investigated using XPS.

Figure 6 shows the Cr 2*p* spectral region for air-dried, heat-treated, and sulfided chromia-pillared montmorillonite. Spectral details are presented in Table 2. In the case of air-dried Cr-PM, the binding energy (BE) of Cr $2p_{3/2}$ is akin to that reported for CrOOH (577.0 eV) (34) (see Fig. 6, spectrum 1, and Table 2), whereas it differs from the BEs measured for CrO_3 (579.8 eV) (34), chromia (576.7–576.9 eV) (34), and homoionic Cr^{3+}-exchanged montmorillonite (578.1 eV). The difference between the Cr 2*p* BEs of air-dried Cr-PM and Cr_2O_3 is due most probably to the strongly hydrated form of the chromia pillars, the presence of which has to be expected (14) and which is confirmed by the TG results described above. Also, it is possible that the polynuclear constitution of the pillars leads to different BEs for the Cr-PM and homoionic Cr^{3+}-exchanged form of clay. Considering these findings, one might suggest that the air-dried material contains chromia pillars having a hydroxymetal form, with trivalent chromium being predominant.

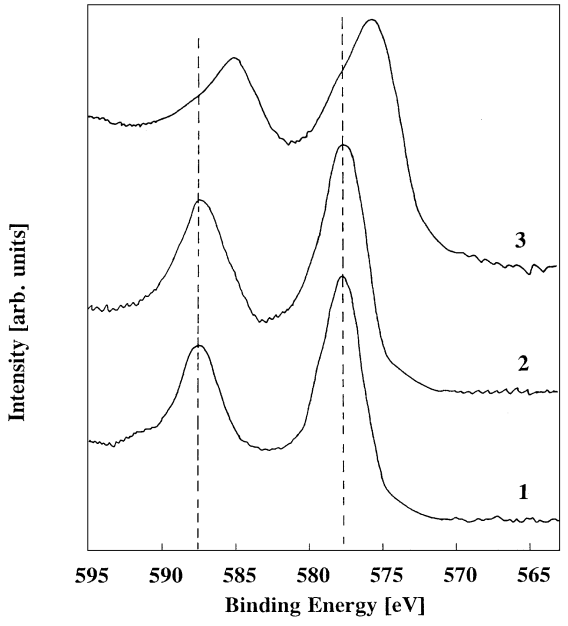

FIG. 6. X-ray photoelectron spectra of the Cr 2*p* region for the Cr-PM sample: (1) air-dried sample, (2) heat-treated at 673 K, (3) sulfided at 673 K.

TABLE 2

Cr 2*p* and S 2*p* Binding Energies and XPS Peak Intensity Ratios of Air-Dried, Modified Cr-PM and Cr^{3+}-Exchanged Clay

Sample	Binding energy (eV)			Intensity ratio	
	Cr $2p_{1/2}$	Cr $2p_{3/2}$	S 2*p*	$I_{Cr\,2p}/I_{Si\,2p}$	$I_{S\,2p}/I_{Cr\,2p}$
Cr-PM	586.9 (4.25)[a]	577.6 (3.70)	—	0.197	—
Cr-PM(He)	586.9 (4.85)	577.4 (3.83)	—	0.197	—
Cr-PM(sulf)	585.1 (5.53)	576.0 (5.06)	162.2 (3.01)	0.194	1.25
Cr^{3+}-exchanged M	587.6 (4.56)	578.1 (4.02)	—	0.015	—

[a] FWHM (eV) in parentheses.

Heat treatment under inert atmosphere of Cr-PM at 673 K does not cause marked changes in the BE and width of the Cr 2*p* peaks, as follows from Fig. 6 (spectra 1, 2) and Table 2. This means that the oxidation state of the chromium present in the pillars was not significantly modified, which is in agreement with the TG data showing that dehydroxylation of the pillars is not completed at 673 K. Therefore, they are most likely to have a hydroxy(oxo)chromium composition. No difference in Cr 2*p*/Si 2*p* intensity ratio was found between the air-dried sample and the heat-treated one, as follows from Table 2. This fact means there are no essential changes in location and/or dispersion of the chromium-containing species.

As shown in Fig. 6 (spectrum 3) and Table 2, the Cr $2p_{3/2}$ BE of the sulfided sample is 1.4 eV lower than that of the heat-treated material an differs from the Cr $2p_{3/2}$ BEs reported for Cr_2S_3 (574.9 eV) and CrS (575.6 eV) (34). This shift reflects a chemical interaction between chromia pillars and sulfiding agent (H_2S–H_2 mixture). The fact that the BE is higher than that reported for metallic chromium (574.0 eV) (34) is consistent with such a suggestion and

provides evidence that Cr is in a positive valence state coordinated by sulfur ligands. That the Cr $2p_{3/2}$ BE determined for the sulfided sample (576.0 eV) is between those of Cr_2O_3 (576.7 eV) and Cr_2S_3 (574.9 eV) could be the result of the pillars' containing Cr(III)-oxysulfide species. Sulfidation also did not result in diminution of the Cr 2*p*/Si 2*p* intensity ratio (see Table 2). Sulfided Cr-PM(He) exhibits significant broadening of the Cr 2*p* XPS peaks (FWHM), as can be seen in Fig. 6 and Table 2. It is reasonable to expect that the change in morphology of the pillared clay aggregates during sulfidation (see SEM images), resulting in differences in local charging, may affect the FWHM. As mentioned above, nitrogen adsorption shows a decrease in micropore volume of the Cr-PM(He) on sulfidation. Comparing these findings, one might conclude that formation of the Cr-sulfide and/or Cr-oxysulfide phase takes place inside the intercrystalline pore system of the pillared clay. The XPS S 2*p* spectrum of Cr-PM(sulf) displays an S $2p_{3/2}$ BE of 162.2 eV (not shown). This value is slightly lower than that found for Cr_2S_3 (162.5 eV) and slightly higher than the value reported for S^{2-} ions (161.0–161.7 eV) (35, 36). Evidence for the presence of elemental sulfur (164.4 eV) or sulfate ions (169.0 eV) has not been found.

The S 2*p*/Cr 2*p* intensity ratio is somewhat lower than that reported for Cr_2S_3 (35). This finding again most likely reflects the existence of some incompletely sulfided chromium ions. Therefore, the data obtained by XPS reveal the complexity of the chemical composition of pillars after sulfidation.

6. *Catalytic Activity*

The results of the activity measurements are presented in Fig. 7. The reaction rate constants for the hydrodesulfurization of thiophene (HDS) and consecutive hydrogenation of butene (HYD) at 623 and 673 K are plotted as a function of the time on stream. The catalysts were tested for 24 h.

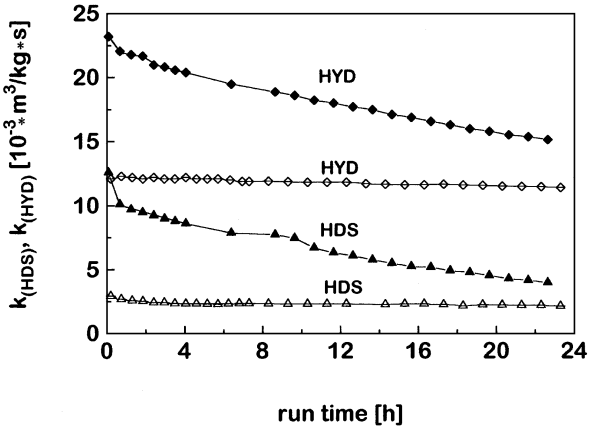

FIG. 7. Thiophene HDS and butene HYD over Cr-PM at 623 K (empty points) and 673 K (filled points).

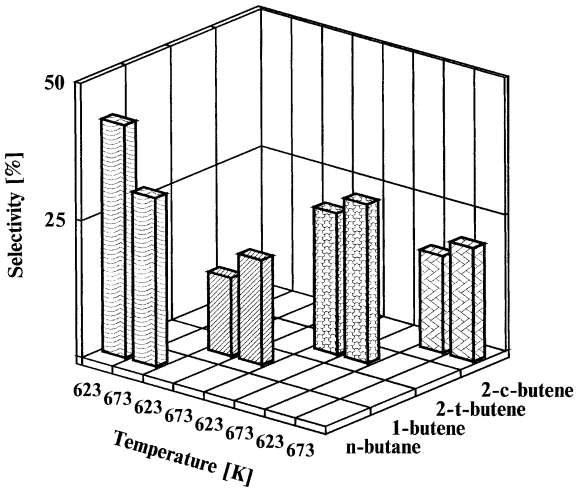

FIG. 8. Product selectivities as a function of thiophene HDS reaction temperature for Cr-PM(sulf) catalyst. Thiophene conversion is equal to 20%.

The Cr-PM(sulf) catalyst deactivates relatively strongly during the first 5 to 35 min of the test experiment, with the strongest deactivation being observed at 673 K. This is probably due to coking, although a contribution to the activity decrease arising from the establishment of a new equilibrium under reaction conditions cannot be excluded (37). The overall deactivation of Cr-PM(sulf) is very small when the thiophene HDS reaction is carried out at 623 K, even when the run time is more than 50 h (not shown); however, also at 673 K, Cr-PM(sulf) deactivates less than carbon-supported Cr-sulfide catalysts (38). In accordance with the findings of Vissers *et al.* (38) and Eijsbouts (39) for Cr-sulfide supported on carbon (4.9% Cr/C), Cr-PM(sulf) showed interestingly high butene hydrogenation activity. Initially, the k_{HYD}/k_{HDS} ratio at 623 K is about twice as high as at 673 K (Fig. 7). From the similarity in hydrogenation activity of the carbon-supported Cr-sulfide catalysts (completely sulfided, relatively low Cr loading) and the pillared montmorillonite-supported catalysts, it might be concluded that the high butene HYD activity is connected to the presence of the same type of Cr-sulfide species, the formation of which does not depend on the type of carrier material and the chromium loading. With respect to selectivity it can be stated that generally thiophene HDS over Cr-PM(sulf) at 623 and 673 K resulted exclusively in the formation of butane and butenes (see Fig. 8). Only during the initial stage of the catalytic test at 673 K (when thiophene conversion was high, more than 60%) could a small amount (less than 7%) of C1–C3 hydrocarbons be detected.

In theory, it is possible that Cr-sulfide sites active for thiophene HDS can be formed by sulfidation of monocationic species located on the external surface of clay sheets. Furthermore, extended interlayers produced by pillaring make the clay interior surface accessible to (large) organic

molecules. Hence, the question arises whether the activity of Cr-PM(sulf) is linked to the presence of chromium (oxy)sulfide pillars or is simply caused by the availability of additional internal surface. An answer to this question can be obtained from a comparison of the catalytic properties of chromium-exchanged (nonpillared) and chromia-pillared montmorillonites.

Sulfided Cr^{3+}-exchanged clay exhibits a low initial thiophene HDS activity (conversion of about 2.5%) associated with a high deactivation rate. Likewise, the HDS specific activity (rate constant related to the surface area) of this sample is more than one order lower than that for Cr-PM(sulf). The same dependence applies to the activity per mole of chromium. Therefore, the contribution of the chromium sulfide species created by Cr^{3+}-exchangeable cations to the high thiophene HDS activity of Cr-PM(sulf) is most probably very small.

Concerning the role of the exposed clay sheets in the formation of the HDS active sites, it is very difficult to imagine that a surface hydroxyl group with low acidity can influence the activity of pillared material to a considerable extent. For instance, Na-exchanged montmorillonite (starting material for Cr-PM preparation) treated under the same conditions as Cr-PM (heating and sulfidation) does not exhibit any thiophene conversion. From the above, and the observation that the HDS activity of nonsulfided chromia-pillared montmorillonite is considerably lower than that of the sulfided form (18), one can conclude that the presence of Cr-sulfide pillars is of prime importance to the high thiophene activity of chromium sulfide-pillared montmorillonite.

CONCLUSIONS

The washing procedure, which probably involves hydrolysis of the hydroxychromium polycations bound to the clay surface, is found to improve the crystallinity of chromia-pillared montmorillonite. Pillaring of montmorillonite with these polycations leads to changes in the surface texture of the clay. The distribution of chromium throughout Cr-PM is practically uniform. The air-dried material contains pillars in a hydroxymetal form, with trivalent chromium being predominant. Cr-PM is partly microporous and partly mesoporous.

Heat treatment at 673 K in an inert atmosphere results in remarkable changes in Cr-PM aggregate morphology indicated by variations in stacking. The broadening of X-ray reflections observed on heating can be attributed, to a large extent, to the formation of partially delaminated aggregates; however, heat treatment does not drastically change the pore structure of Cr-PM, the distribution of chromia pillars, or the chromium oxidation state.

Sulfidation of Cr-PM(He) does not strongly modify the basal spacing of the material but does influence the aggregate morphology. On sulfidation the oxidic pillars are converted into the Cr(III)-sulfide and/or oxysulfide form, as evidenced by XPS. Sulfur is found to be present as almost uniformly distributed S^{2-}. No indications of the presence of SO_4^{2-} or elemental sulfur have been observed. Sulfidation does not cause marked sintering and/or displacement of the pillars inside the interlamellar space of Cr-PM. Thus it can be stated that sulfidation under the conditions applied does not significantly change the pore structure of Cr-PM which persists with virtually no collapse. The chromium sulfide-pillared montmorillonite obtained has a high specific surface area and a micro/mesoporous structure.

The high thiophene HDS and butene hydrogenation activities of Cr-PM(sulf) are clearly related to the presence of chromium sulfide pillars.

ACKNOWLEDGMENTS

The authors thank Mr. M. W. G. M. Verhoeven for XPS measurements and Dr. N. Kostoglod for her help. These investigations were supported in part by The Netherlands Foundation for Chemical Research (SON) with financial aid from The Netherlands Technology Foundation (STW) and in part by the Ukrainian State Committee for Science and Technology (DCNT).

REFERENCES

1. Prins, R., de Beer, V. H. J., and Somorjai, G. A., *Catal. Rev. Sci. Eng.* **31**, 1 (1989).
2. Delmon, B., *Catal. Lett.* **22**, 1 (1993).
3. Maxwell, I. E., *Catal. Today* **1**, 385 (1987).
4. Ward J. W., *Stud. Surf. Sci. Catal.* **16**, 587 (1983).
5. Cid, R., Orellana, F., and Lopez Augusto, A., *Appl. Catal.* **32**, 327 (1987).
6. Thomas, J. M., and Theocharis, C. R., *in* "Perspectives in Catalysis" (J. M. Thomas and K. I. Zamaraev, Eds.), p. 465. Blackwell, London, 1992.
7. Yamanaka, S., and Takahama, K., *in* "Multifunctional Mesoporous Inorganic Solids" (C. A. C. Sequeira and M. J. Hudson, Eds.), p. 237. Kluwer Academic, Dordrecht/Norwell, MA, 1993.
8. Schoonheydt, R. A., *Stud. Surf. Sci. Catal.* **58**, 201 (1991).
9. Burch, R., and Warburton, C. I., *J. Chem. Soc. Chem. Commun.*, 117 (1987).
10. Warburton, C. I., *Catal. Today* **2**, 271 (1988).
11. Rightor, E., Tzou, M.-S., and Pinnavaia, T. J., *J. Catal.* **130**, 29 (1991).
12. Occelli, M. L., and Rennard, R. J., *Catal. Today* **2**, 309 (1988).
13. Kloprogge, J. T., Welters, W. J. J., Booy, E., de Beer, V. H. J., van Santen, R. A., Geus, J. W., and Jansen, J. B. H., *Appl. Catal. A* **97**, 77 (1993).
14. Tzou, M.-S., and Pinnavaia, T. J., *Catal. Today* **2**, 243 (1988).
15. Pinnavaia, T. J., Tzou, M.-S., and Landau, S. D., *J. Am. Chem. Soc.* **107**, 4783 (1985).
16. Auer, H., and Hofmann, H., *Appl. Catal. A* **97**, 23 (1993).
17. Bradley, S. M., and Kydd, R. A., *J. Catal.* **141**, 239 (1993).
18. Sychev, M., de Beer, V. H. J., van Santen, R. A., Prohod'ko, R., and Goncharuk, V., *Stud. Surf. Sci. Catal.* **84**, 267 (1994).
19. Brindley, G. W., and Yamanaka, S., *Am. Mineral.* **64**, 830 (1979).
20. Jimenez-López, A., Maza-Rodriguez, J., Olivera-Pastor, P., Maireles-Torres, P., and Rodriguez-Castellon, E., *Clays Clay Miner.* **41**, 328 (1993).

21. Sychev, M., de Beer, V. H. J., and van Santen, R. A., *Microporous Mater.*, **8**, 255 (1997).
22. Nemecz, E., "Clay Minerals." Akadémiai Kiadó, Budapest, 1981.
23. Shirley, D. A., *Phys. Rev. B* **5**, 4750 (1972).
24. Scofield, J. H., *J. Electron Spectrosc. Relat. Phenom.* **8**, 129 (1976).
25. Duchet, J. C., van Oers, E. M., de Beer, V. H. J., and Prins R., *J. Catal.* **80**, 386 (1983).
26. Vaughan, D. E. W., *Catal. Today* **2**, 187 (1988).
27. Pinnavaia, T. J., Tzou, M.-S., Landau, S. D., and Raythatha, R. H., *J. Mol. Catal.* **27**, 195 (1984).
28. Brunauer, S., Deming, L. S., Deming, W. S., and Teller, E., *J. Am. Chem. Soc.* **62**, 1723 (1940).
29. Theocharis, C. R., *in* "Multifunctional Mesoporous Inorganic Solids" (C. A. C. Sequira and M. J. Hudson, Eds.), NATO ASI Series, p. 3. Kluwer Academic, Dordrecht/Norwell, MA, 1993.
30. Gregg, S. J., and Sing, K. S. W., "Adsorption, Surface Area and Porosity," 2nd ed. Academic Press., London, 1982.
31. Burch, R., and Warburton, C. I., *J. Catal.* **97**, 503 (1986).
32. Malla, P., and Komarneni, S., *in* "Proceedings, 9th International Clay Congress" (V. C. Farmer and Y. Tardy, Eds.). *Sci. Geol. Mem.* **86**, 59 (1990).
33. Volzone, C., Cesio, A. M., Tores Sanchez, R. M., and Pereira, E., *Clays Clay Miner.* **41**, 702 (1993).
34. Moulder, J. F., Stickle W. F., Sobol P. E., and Bomben, K. D., "Handbook of X-ray Photoelectron Spectroscopy" (J. Chastain, Ed.), p. 213. Perkin–Elmer, MN, 1992.
35. De Jong, A. M., Thesis, Eindhoven University of Technology, Eindhoven, 1994.
36. Bouwer, S. M. A. M., van Zon, F. B. M., van Dijk, M. P., van der Kraan, A. M., de Beer, V. H. J., van Veen, J. A. R., and Koningsberger, D. C., *J. Catal.* **146**, 375 (1994).
37. De Beer, V. H. J., Bevelander, C., van Sient Fiet, T. H. M., Werter, P. G. A. J., and Amberg, C. H., *J. Catal.* **43**, 68 (1976).
38. Vissers, J. P. R., Groot, C. K., van Oers, E. M., de Beer V. H. J., and Prins, R., *Bull. Soc. Chim. Belg.* **93**, 813 (1984).
39. Eijsbouts, S., Thesis, Eindhoven University of Technology, Eindhoven, 1989.